CROSS-FLOOR VIBRATION WAVE PROPAGATION IN HIGH-RISE COMPOSITE：A CASE STUDY ON AN INDUSTRIAL BUILDING

Ruoyang Zhou

School of Intelligent Civil and Ocean Engineering, Harbin Institute of Technology, Shenzhen
Shenzhen, 518000, China
ruoyangchou@163.com

Xiaoxiong Zha

School of Intelligent Civil and Ocean Engineering, Harbin Institute of Technology, Shenzhen
Shenzhen, 518000, China
zhaxx@hit.edu.cn

Jianqiao Ye*

School of Engineering, Lancaster University, Bailrigg, Lancaster LA1 4YW
Lancaster, LA1 4YW, United Kingdom
j.ye2@lancaster.ac.uk

Received Day Month Year
Revised Day Month Year

High-rise steel–concrete composite structures are particularly susceptible to vibration-induced comfort issues, which can negatively impact both the health and productivity of on-site workers and office staff. In contrast to the study that are currently available in the literature, which are mostly on vibration responses of individual structural components, a new calculation method using vibration wave propagation (WPA) is proposed, calibrated and validated in this study to predict peak accelerations of any locations anywhere in a building due to an excitation that can be floors away. On-site vibration tests are also conducted on an existing high-rise steel–concrete composite building built for shared factory space and offices. The results of the tests are used to validate the theoretical calculation method. For easier implementation in practical design calculation, a simplified equation of vibration wave propagation is proposed based on data regression. The parameters of the equation are determined by fitting the data from the theoretical calculations. The derived regression equation enables the prediction of peak vibration accelerations of a floor slab under an excitation on the same floor, or on a different floor. This capability enables the possibility of optimizing equipment layout and improving vibration control in high-rise steel–concrete composite industrial buildings.

Keywords: Steel-concrete composite structure; high-rise industrial building; wave propagation analysis; vibration peak acceleration.

1. Introduction

High-rise buildings, which allow major cities to accommodate more people and industrial plants, are amongst the most important infrastructure of modern urbanization. Particularly,

high-rise multifunctional buildings that combine office, research and industrial production spaces have become increasingly popular in China. In this type of building, vibration waves generated by equipment installed on the middle or upper floors propagate to all parts of the building and may cause serious health issues to the people working in both the production and office areas. For example, the Pingshan new energy vehicle industrial building shown is Fig. 1 was built from concrete-filled steel tubular columns, steel beams, and reinforced truss floor slabs. The building consists of 15 floors and is 100m in height. Its designed functional areas include spaces for offices, automotive research and development, and automobile manufacturing.

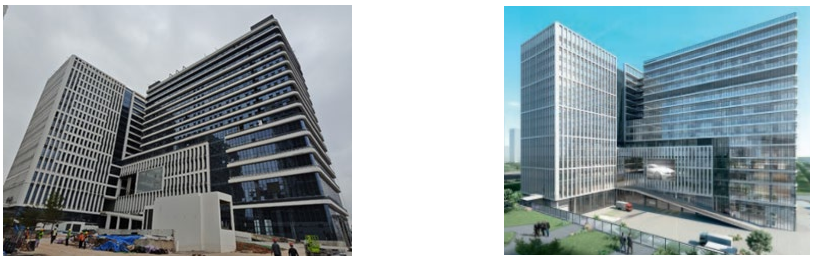

a) Completed construction of the industrial building b) Rendering of the completed industrial building

Fig. 1 Pingshan new energy vehicle industrial building

However, the propagation of vibration waves generated by equipment is often not a primary consideration, especially in these tall, mixed-use buildings in current design practices. There is also a lack of theoretical or numerical tools that can accurately predict vibration wave propagation in multi-story steel–concrete composite structures. Clearly, there is an urgent industrial demand for systematic research on this emerging topic, since more high-rise industrial buildings are expected to be constructed in the coming decade. The lack of design tools for predicting structural vibrations of modern multifunctional industrial building has to be addressed.

Compared to traditional multi-story industrial buildings, modern high-rise steel–concrete composite industrial buildings often exceed ten floors and rise above 30 meters, with some reaching up to 100 meters. In many cases, large industrial equipment is installed in the middle or upper sections, raising the center of gravity of a building and intensifying vibration-related issues.[1] These factors make equipment-induced vibration a critical concern, emphasizing also the urgent need for more accurate theoretical models and practical design approaches to manage vibration in such structures.

Extensive studies have examined vibration issues in traditional low-rise and multi-story industrial buildings. Gasella conducted numerical simulations on individual structural component to evaluate equipment-induced translational and torsional vibrations, and to identify peak response locations.[2] Li and Peng carried out on-site dynamic test and computer simulations on individual structural component to analyze resonance effects when structural natural frequencies approach the equipment excitation frequency.[3] Carlson and Spencer applied perturbation methods to investigate the impact of equipment vibrations on low-stiffness, small-damping individual structural component.[4] Lung proposed a modified response spectrum calculation method on individual structural component for cases where equipment and structural frequencies are close to each other.[5] Furthermore, Gerardo and Amador showed that when the excitation period coincides with a higher-order mode, the resulting resonance can markedly amplify responses in the higher level of stories even if the harmonic load is applied to all floors, underscoring the need to account for higher-mode participation in cross-floor vibration assessment.[6] Wu and Pu et al demonstrated through shake-table tests that local stiffening at the equipment floor fails to suppress far-field responses once higher-mode resonance is activated, reinforcing the importance of a system-level mitigation strategy.[7] Li and Zhang's large-scale finite-element study revealed that adding secondary beams beneath vibrating machinery reduced local accelerations by less than 10 % but left upper-story responses virtually unaffected, further underscoring the need for holistic, building-wide damping solutions.[8]

Researchers have applied various methods, including the transfer function method, transfer matrix method, impedance synthesis method, admittance method, spectral analysis method, and the wave propagation analysis (WPA) method in their research. Among these, the WPA method offers distinct advantages in handling boundary and constraint conditions while ensuring the mathematical formulation remains clear. Wu and Mead developed a WPA method for bending waves in multi-support Bernoulli–Euler beams,[9] Tso and Hansen extended it to wave transmission in plates and cylinders.[10] Subsequent studies by Qin and Zeng,[11] Chen and Zhang,[12] and Zhou et al.[13] applied the WPA method to more complex structures. Despite these advancements, the current WPA applications primarily focus on individual slabs or columns, with only limited studies addressing vibration wave propagation in entire high-rise structures.[14]

In this study, the WPA method is extended to analyze vibration waves in a high-rise steel–concrete composite industrial building. The propagation of vibration waves in beams, columns and slabs of the same floor is considered. The propagation across floors is studied by considering wave propagation through slab-column joints. A new calculation method and regression equations for vibration wave propagation are proposed, which is validated against on-site test results of the building (Fig. 1). The developed approach enables theoretical prediction of structural responses at any locations within the building due to the vibration excitations from any other positions of the same building.

2. The calculation theory of the WPA method

2.1. *A brief review on WPA method*

2.1.1. *Forced vibration of a rectangular plate structure with simply supported on all four edges*

Consider a simply supported rectangular plate, that is a typical model of a concrete floor slab. The four edges of the slab are defined by $x = 0$, $x = L_x$, $y = 0$ and $y = L_y$, respectively. The coordinate system and boundary conditions are shown in Fig. 2. It is assumed that the following pressure wave load $\tilde{W}(x, y, t)$ acts on the surface of the plate,[14] which is

$$\tilde{W}(x, y, t) = \sum_{m}^{\infty} W_m \sin(k_{my} y) e^{j(\omega t - k_p x)}, \tag{2.1}$$

where W_m is the amplitude of a pressure wave; $k_{my} = m\pi / L_y$ represents the wave number in the y-direction; ω is the circular frequency of the pressure wave; k_p is the wave number in the x-direction of the pressure wave, and t denotes time.

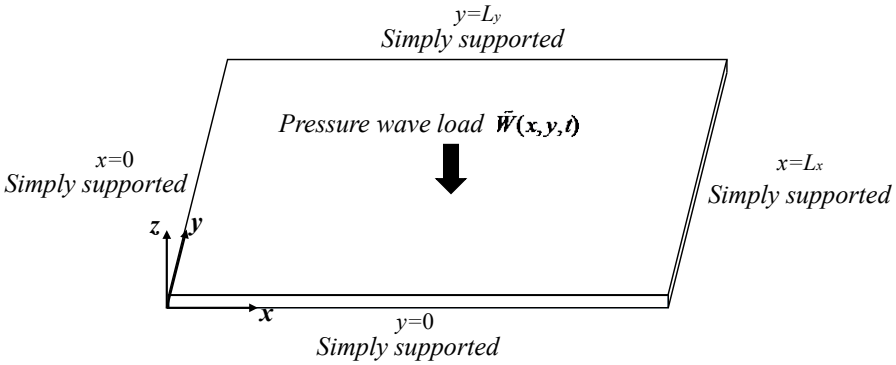

Fig. 2 Simply supported rectangular plate and applied pressure load.

Eq. (2.1) represents the propagation of a vibrational pressure wave along the x-direction, with a propagation speed, v_p, of

$$v_p = \frac{\omega}{k_p}. \tag{2.2}$$

We consider the case when the half-wave length of the pressure is equal to the length of the plate in the y-direction. Thus,

$$\tilde{W}(x,y,t) = W_1 \sin(k_{1y} y) e^{j(\omega t - k_p x)}. \tag{2.3}$$

The displacement of the plate, $w_p(x,y,t)$, satisfy the following equation

$$D\nabla^4 w_p(x,y,t) + \rho h \omega^2 w_p(x,y,t) = W_1 \sin(k_{1y} y) e^{j(\omega t - k_p x)}, \tag{2.4}$$

where D is the bending stiffness of the plate; ρ is the density of the plate; h is the thickness of the plate. By assigning a complex bending stiffness $D(1+j\tau)$, the internal damping of the plate can be considered, where τ is the damping loss factor.

The solution of Eq. (2.4) consists of two parts: the particular solution and the complementary solution. The particular solution w_1 represents the response in the longitudinal direction of an infinitely long plate, i.e., the propagation of waves in the x-direction if it is sufficiently long. For a plate of finite length, the wave w_2 will be reflected when they propagate and encounter the plate boundaries.

Therefore, the total displacement $w_p(x,y,t)$ can be expressed as

$$w_p(x,y,t) = w_1 + w_2 = \frac{W_1 \sin(k_{1y}y)e^{j(\omega t - k_p x)}}{D(k_{1y}^2 + k_p^{\ 2}) - ph\omega^2} + (A_1 e^{k_n x} + A_2 e^{-k_n x} + A_3 e^{jk_x x} + A_4 e^{-jk_x x})\sin(k_{1y}y)e^{j\omega t}$$
$$= \left[A_1 e^{k_n x} + A_2 e^{-k_n x} + A_3 e^{jk_x x} + A_4 e^{-jk_x x} + \frac{W_1 e^{-jk_p x}}{D(k_{1y}^2 + k_p^2) - ph\omega^2} \right] \sin(k_{1y}y)e^{j\omega t}, \quad (2.5)$$

where $k_n^2 = k^2 + k_{1y}^2, k_x^2 = k^2 - k_{1y}^2$, A_n is an unknown coefficient.

The solution includes four unknowns, which can be determined by satisfying the four boundary conditions. For the case of simply supported edges, the boundary conditions are

$$\left.\begin{aligned} w &= 0 \\ \frac{\partial^2 w}{\partial x^2} &= 0 \end{aligned}\right\} \quad (2.6)$$

at $x = 0$ and $x = L_x$

$$\left.\begin{aligned} w &= 0 \\ \frac{\partial^2 w}{\partial y^2} &= 0 \end{aligned}\right\} \quad (2.7)$$

at $y = 0$ and $y = L_y$.

The four unknown constants, A_n (n = 1, 2, 3 and 4), can be obtained by solving Eq. (2.8)

$$\begin{bmatrix} 1 & 1 & 1 & 1 \\ k_n & -k_n & jk_x & -jk_x \\ e^{k_n L_x} & e^{-k_n L_x} & e^{jk_x L_x} & e^{-jk_x L_x} \\ k_n e^{k_n L_x} & -k_n e^{-k_n L_x} & jk_x e^{jk_x L_x} & -jk_x e^{-jk_x L_x} \end{bmatrix} \begin{Bmatrix} A_1 \\ A_2 \\ A_3 \\ A_4 \end{Bmatrix}$$
$$= \begin{Bmatrix} 1 \\ -jk_p \\ e^{-jk_p L_x} \\ -jk_p e^{-jk_p L_x} \end{Bmatrix} \frac{W_1}{D(k_{1y}^2 + k_p^2) - \rho h\omega^2}. \quad (2.8)$$

Therefore, for given k_p and ω, the displacement at any point on the plate can be expressed as

$$w_p(x,y,t) = Y(x,y,k_p,\omega)W_1 e^{j\omega t}, \quad (2.9)$$

where $Y(x,y,k_p,\omega)$ represents the wave response function.

By taking the first and second derivatives of Eq. (2.9) with respect to t, the velocity and acceleration of the plate can be obtained.

2.1.2. *Forced longitudinal vibration of a column with clamped ends*

Consider a homogeneous column of length L with a uniform cross-section of area S, material density ρ, and Young's modulus E. It is assumed that the cross-section remains planar during vibration and that the transverse deformation is negligible. As a result, all points on the same cross-section undergo identical longitudinal displacements in the z-direction. Hence, the differential equation for the free longitudinal vibration of the column is[15]

$$\frac{\partial^2 w_c(z,t)}{\partial z^2} = \frac{1}{c_L^{\,2}} \frac{\partial^2 w_c(z,t)}{\partial t^2}, \tag{2.10}$$

where $c_L = \sqrt{E/\rho}$ represents propagation speed of longitudinal waves. The free vibration wave, $w_c(z,t)$, expressed using a complex exponential form, is

$$w_c(z,t) = Ae^{j\omega t - jkz} + Be^{j\omega t + jkz} = (Ae^{-jkz} + Be^{jkz})e^{j\omega t}, \tag{2.11}$$

where A and B are unknown coefficients; k is the wave number of the pressure wave; ω is the circular frequency of the pressure wave.

The equation for forced longitudinal vibration of a column under external load $F(z,t)$ is

$$\rho S \frac{\partial^2 w_c(z,t)}{\partial t^2} = ES \frac{\partial^2 w_c(z,t)}{\partial z^2} + F(z,t). \tag{2.12}$$

Let $F(z,t) = F(z)e^{j\omega t}$, then $w_c(z,t) = w_c(z)e^{j\omega t}$. The differential equation for forced longitudinal vibration of the column becomes

$$\frac{d^2 w_c(z)}{dz^2} + \frac{\omega^2}{c_L^{\,2}} w_c(z) = -\frac{1}{ES} F(z). \tag{2.13}$$

When a harmonic longitudinal force is applied to a finite-length column, two-way waves are generated, which propagate along the column in opposite direction. These waves reflect at the ends of the column, generating two additional waves travelling also in the longitudinal direction. Thus, the longitudinal displacement $w_c(z)$ of the column at a given moment can be represented by superposition of the four waves using the WPA as[12]

$$w_c(z) = (Ae^{-jkz} + Be^{jkz}) + \frac{F_0}{4ESk_L} j\left[e^{jk_L|z-z_0|} - e^{-jk_L|z-z_0|}\right], \tag{2.14}$$

where A and B are unknown coefficient; k is the wave number of the pressure wave; F_0 is the amplitude of the harmonic force; S is the cross-sectional area; $k_L = \omega/c_L = \omega\sqrt{\rho/E}$; z_0 is the position of action of the harmonic force.

Assume that the column is clamped at both ends, which is typical support conditions for load bearing columns in high-rise buildings. The boundary conditions that must be satisfied at both $z = 0$ and $z = L$ are

$$\left.\begin{aligned} w_c &= 0 \\ \frac{\partial w_c}{\partial z} &= 0 \end{aligned}\right\}. \tag{2.15}$$

The introduction of the above boundary conditions results in the following two equations for A and B

$$\begin{bmatrix} 1 & 1 \\ e^{-jkL} & e^{jkL} \end{bmatrix} \begin{Bmatrix} A \\ B \end{Bmatrix} = -\frac{W_0}{4ESk_L} j \begin{Bmatrix} e^{jk_L|z_0|} - e^{-jk_L|z_0|} \\ e^{jk_L|L-z_0|} - e^{-jk_L|L-z_0|} \end{Bmatrix}. \tag{2.16}$$

2.2. *Calculation of vibration wave propagation in a building*

2.2.1. *Calculation of vibration wave propagation across a single floor*

Part or all of the waves travelling in a structure will reflect during propagation when meeting discontinuities and generate near-field waves on the reflecting interface. Some of the wave energy “transmits” across the discontinuities, and continues to propagate.

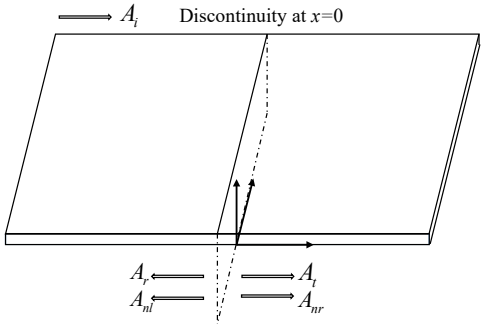

Fig. 3 Wave propagation in the discontinuous plate

Assume that the uniform plate structure shown in the Fig. 3 is discontinuous at $x = 0$. The incident pressure wave $\tilde{A}_i$ in the region where $x < 0$ is

$$\tilde{A}_i = A_i e^{j(\omega t - kx)}, \tag{2.17}$$

where A_i represents the amplitude of the pressure wave; ω is the circular frequency of the pressure wave; k is the wave number of the pressure wave.

Similarly, structural wave reflection and transmission occur at $x = 0$. The reflected wave can be expressed as $\tilde{A}_r$, and the near-field wave generated from the reflection interface is $\tilde{A}_{nl}$. The transmitted propagation wave and the near-field wave in the region where $x > 0$ are respectively, $\tilde{A}_t$ and $\tilde{A}_{nr}$.

Therefore, the displacements, w_{p+} and w_{p-}, of the plate on the left-and right-hand sides of the discontinuity can be described as

$$\left.\begin{aligned} w_{p+} &= (A_t e^{-jkx} + A_{nr} e^{-kx}) e^{j\omega t} \, (x \geq 0) \\ w_{p-} &= (A_i e^{-jkx} + A_r e^{jkx} + A_{nl} e^{kx}) e^{j\omega t} \, (x < 0) \end{aligned}\right\}, \tag{2.18}$$

where A_r represents the amplitude of the reflected wave; A_{nl} represents the amplitude of the reflected near-field wave; A_t and A_{nr} are the amplitudes of the transmitted propagating wave and the near-field wave, respectively.

Based on the solutions in Section 2.1.1, a MATLAB code is formulated to calculate the propagation of vibration waves across a single floor. The boundary conditions along the outside beams are treated as simply supported edges (marked black in Fig. 4). All the internal beams provide intermediate supports to the slab (marked yellow in Fig. 4).

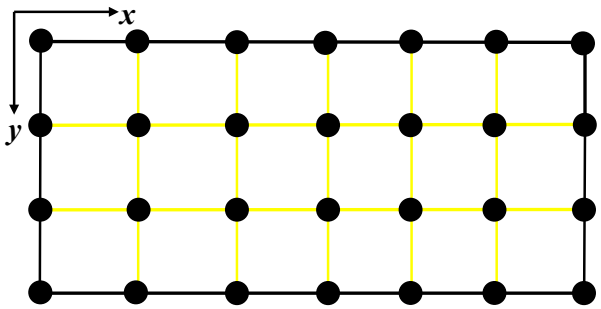

Fig. 4 Schematic diagram of theoretical calculation boundary conditions

Consider wave propagation in a plate with a simply supported edge at the end, as shown in Fig. 5a, where both displacement $w_p(0)$ and bending moment $M_+(0)$ and $M_-(0)$ must be zero. Two reflected wave amplitudes A_r and A_{nl} can be obtained, which are as follows

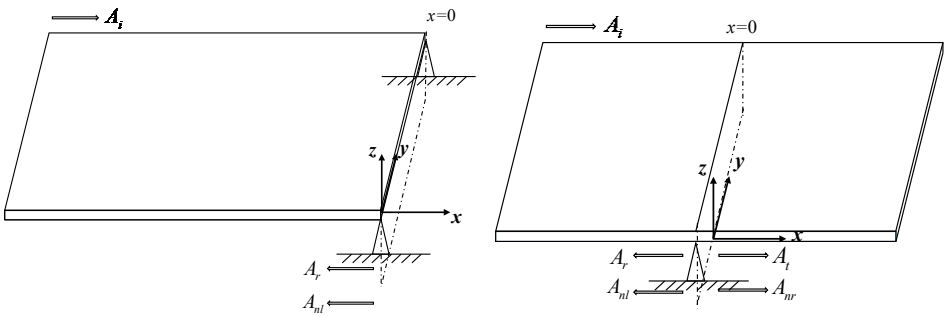

a) with a simply supported edge at the end b) with an intermediate supported at the middle span

Fig. 5 wave propagation in a plate

$$\left.\begin{aligned} A_r &= -A_i \\ A_{nl} &= 0 \end{aligned}\right\}. \tag{2.19}$$

Consider the wave propagation in the plate with an intermediate support at the middle span, as shown in Fig. 5b. Both displacement $w_{p+}(0)$ and $w_{p-}(0)$ and bending moment $M_+(0)$ and $M_-(0)$ must be zero. Four structural wave amplitudes, A_r, A_{nl}, A_t and A_{nr} can be obtained, which are as follows

$$\left.\begin{aligned} A_r &= -j\frac{A_i}{1-j} \\ A_t &= j\frac{A_i}{1-j} \\ A_{nl} &= A_{nr} = -jA_r \end{aligned}\right\}. \tag{2.20}$$

2.2.2. *Calculation of vibration wave propagation across different floors*

As described above, vibrational waves are generated under external load and then propagate across the floor. For slab–column connection, the resultant force $F_1(t)$ at the column base is obtained by integrating the normal stress distribution in the floor slab as follows

$$F_1(t) = \int_S \sigma(x,y,t)dS = \int_S E\frac{\partial w_p(x,y,t)}{\partial y}dS\,, \tag{2.21}$$

where $\sigma(x,y,t)$ is the contact stress between the column end and the floor slab; S is the cross sectional area of the column; E is the Young's modulus of the floor slab; $w_p(x,y,t)$ is the displacement of the floor slab in the slab-column contact area.

Assume that floor B is the source of vibration, Fig. 6 schematically illustrates how the force is transmitted from floor B to floor A through a slab-column connections, where $F_1(t)$ and $F_2(t)$ represent, respectively, the axial force (load) acting at the bottom end of the column of floor B and the top end of the column of floor A. Eq. (2.21) can be used to calculates the resultant force, $F_1(t)$, at the bottom end slab-column connection of floor B. The force is simultaneously transmitted to the top end of the column of floor A, which is denoted by $F_2(t)$.

Considering the relatively low stiffness of the slabs in comparison to the axial stiffness of the columns, the force in the column of floor B is considered to be fully transmitted to the column of floor A, i.e., $F_1(t)$=$F_2(t)$.

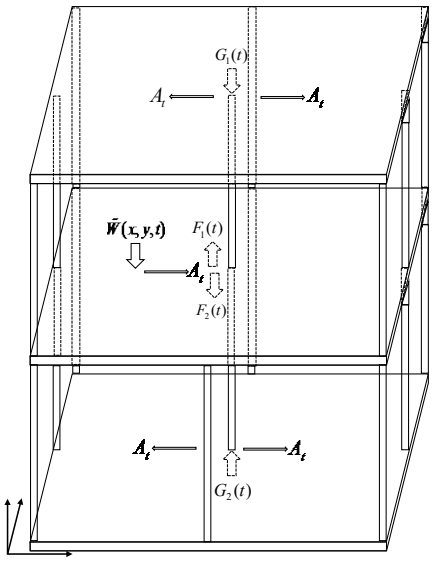

Fig. 6 Vibration wave propagation across different floors

The forces, $F_1(t)$ and $F_2(t)$, propagate along their respect column axis in the opposite direction. The transmitted force of $F_1(t)$ at the top end of the column of floor B is denoted

by $G_1(t)$, and transmitted force of $F_2(t)$ at the bottom end of the column of floor A is denoted by $G_2(t)$.

The propagation of the longitudinal waves in the columns satisfy Eq. (2.10). Due to the time delay in force transmission within the column, the solution of Eq. (2.10) can be expressed as a single-variable function

$$w_c(z,t) = f(\xi), \tag{2.22}$$

where $\xi = t - z/c_L$.

By substituting Eq. (2.22) into Eq. (2.10), the following equation is obtained

$$\frac{d^2 f}{d\xi^2} = \frac{1}{c_L^2} c_L^2 \frac{d^2 f}{d\xi^2} = \frac{d^2 f}{d\xi^2}. \tag{2.23}$$

Clearly, the equation satisfies the consistency condition. Therefore, the solution of Eq. (2.10) can be any function propagating along the $t - z/c_L$.

Since the one-dimensional wave equation is a second-order partial differential equation, its general solution should include two independent solutions. Assuming the solution is the sum of two independent functions, which is

$$w_c(z,t) = f_1(t - z/c_L) + f_2(t + z/c_L), \tag{2.24}$$

where $f_1(t - z/c_L)$ represents the upward-propagating wave in the column of floor B; $f_1(t + z/c_L)$ represents the downward-propagating wave in the column of floor A.

Therefore, an upward-propagating wave is generated when the external force $F_1(t)$ is applied at the bottom end of the column, which is

$$w_c(z,t) = f_1(t - z/c_L), \tag{2.25}$$

the wave reaches the top of the column when $t = L/c_L$ at $z = L$.

The stress and velocity of the column satisfy the following relationship

$$\sigma = Z_{column} \dot{w}_c, \tag{2.26}$$

where $Z_{column} = \rho c_L S$, representing the wave impedance of the column; $\dot{w}_c = \partial w_c / \partial t$ denotes the velocity of a particle within the column.

At the bottom end of the column of floor B, i.e., at $z = 0$, the relationship between the resultant force and velocity is given by

$$F_1(t) = Z_{column} \dot{w}_c(0,t), \tag{2.27}$$

where

$$\dot{w}_c(z,t) = \frac{\partial}{\partial t} f_1(t - z/c_L)\,. \tag{2.28}$$

Thus, the velocity at the top end of the floor B column is the time-delayed form of the velocity at the bottom end of the column.

Due to the effect of damping in the column, the resultant force at the top of the column on floor B, $G_1(t)$, is given by

$$\begin{aligned} G_1(t) &= Z_{column}\dot{w}_c(L,t)e^{-\eta L} \\ &= Z_{column}\dot{w}_c(0,t-L/c_L)e^{-\eta L} = F_1(t-L/c_L)e^{-\eta L}\,, \end{aligned} \tag{2.29}$$

where $\eta = \dfrac{\omega}{2\pi f}\tan(\delta)$, and δ is the damping loss factor.

Similarly, the resultant force at the bottom end of the column on floor A, $G_2(t)$, can be calculated by following the procedure from Eq. (2.22) to Eq. (2.29).

The calculated $G_1(t)$ and $G_2(t)$ serve as the forces acting on the ceiling slab of floor B and the floor slab of floor A, respectively. This enables the calculation of vibration wave propagation through slabs of different floors. Hence, the vibration response of a multiple floor building due to the excitation from a particular floor can be studied by repeating the above solution process progressively until the waves have reached the top and the bottom of the building.

The calculation procedure described above is summarized below in Fig. 7.

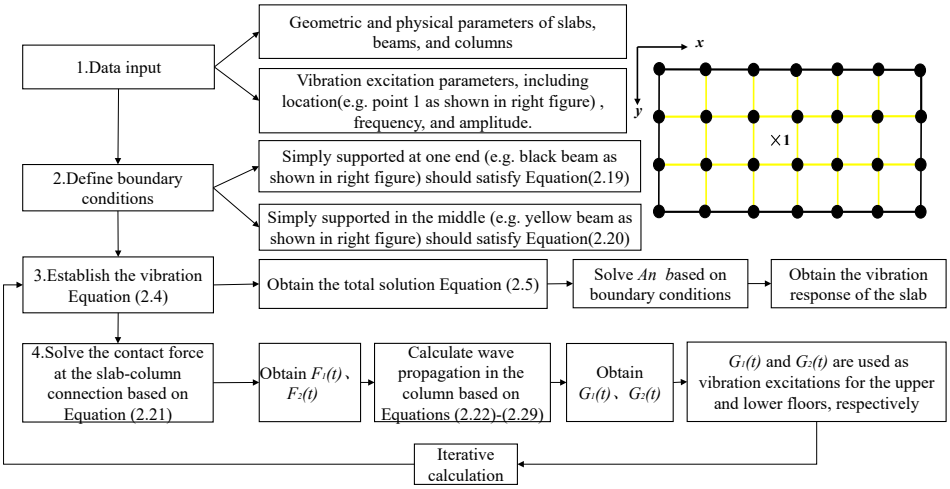

Fig. 7 Calculation procedure of this method

3. Vibration wave propagation test in high-rise building of composite structure

3.1. *Vibration wave propagation test*

Vibration wave tests were carried out on the steel-concrete composite building shown in Fig. 8b The building is 100 meters in height, having 2 underground floors. The industrial building is divided into two zones, A and B, as shown in Fig. 8a, where Zone A is the industrial area, and Zone B is the office area. Zone A has 13 floors and Zone B has only 10 floors. Floors 1-10 of the building are occupied by both factories and offices, while floors 11-13 are all factories. Q355B structural steel was used in the building. The steel has a yield strength of 355 MPa, an ultimate tensile strength of 470–630 MPa, an elastic modulus of 2.0×10^{11} Pa, a Poisson's ratio of 0.3, and a density of 7850 kg/m^3. All the floor beams are steel beams of grade Q355B. The columns are steel tubes filled with concrete, of which the steel is of grade Q355B and the concrete is C60. The thickness of the steel tube is 10mm, and the column diameter is 700mm. The floor slabs are reinforced truss floor slabs, of which the concrete is C30, and the slab thickness is 130mm.

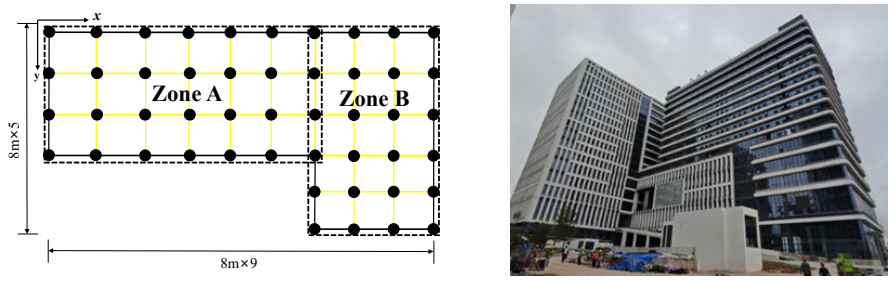

a) Structural layout plan b) Pingshan new energy vehicle industrial building 3A

Fig. 8 Overall structural diagram

To simulate vibrations excited by machines in the industrial zone, the Dongguan Shuangyi vibrator shown in Fig. 9a was used as vibration exciter placed in Zone A, which can generate a sinusoidal excitation force of 3.5 kN, with a vibration frequency adjustable in the range of 0-50 Hz. The signal acquisition sensor used was the Donghua 1A401E, as shown in Fig. 9b, that utilizes high-sensitive piezoelectric ceramics. The Donghua DH8303 dynamic signal test and analysis system, as shown in Fig. 9c, was used to capture and process the signals. During data acquisition, the sampling frequency was set to 1000 Hz, and the sensitivity was set to 5.183 mV/m/s^2.

a) Attachment-type vibrator b) 1A401E sensor c) Dynamic signal acquisition

Fig. 9 Vibration devices applied in the test setup

3.2. *Vibration wave propagation test conditions*

3.2.1. *Modal test conditions*

Heel-drop tests were conducted first to determine the natural frequencies and damping of the floor slabs, as shown by the on-site setup in Fig. 10. For the heel-drop tests, points 16-18 (Zone A) on the 3rd, 8th and 13th floors and points 38-40 (Zone B) on the 3rd, 8th floors, was chosen as the test locations, as shown in Fig. 11.

These floors were chosen to represent lower, mid-height, and upper portions of the building, respectively, and to ensure that any variations in dynamic behaviour across the height of the building were captured. The test points near the mid-span of the floor slabs, where flexural vibrations are typically most pronounced, helped to identify the dominant floor modes and obtain higher signal amplitude for damping and frequency estimation.

Fig. 10 Heel-drop test

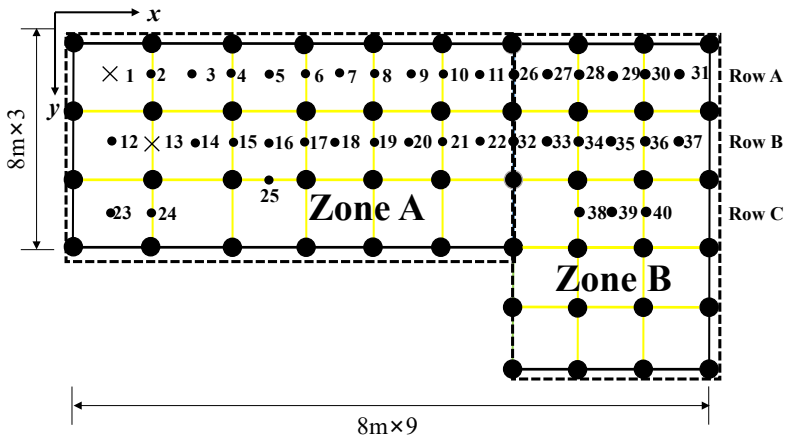

Fig. 11 Measurement point layout

3.2.2. *Vibration test conditions*

To study the propagation of vibration waves across a single floor, the following tests were conducted under conditions 1 and 2 below.

Condition 1: the equipment vibration frequency was set to 50 Hz. The equipment excitation was applied sequentially at point 1 on the 3rd, 8th and 13th floors (at the mid-span of the floor). The sensors were sequentially placed at points 1-12 and 23 on the 3rd, 8th and 13th floors (Zone A) and points 26-31 on the 3rd and 8th floors (Zone B), respectively, as shown in row A and row B in Fig. 13, where the acceleration time history was recorded.

Condition 2: the equipment vibration frequency was set to 50 Hz. The equipment excitation was applied sequentially at point 13 on the 3rd, 8th and 13th floors (at the mid-span of the main beam). The sensors were sequentially placed at points 2, 13-22, and 24 on the 3rd, 8th and 13th floors (Zone A) and points 32-37 on the 3rd and 8th floors (Zone B), respectively, as shown in row B and row C in Fig. 13, where the acceleration time history was collected.

To investigate the influence of excitation location on the vibration response, two groups of excitation positions were chosen: (1) at the mid-span of the main beam (e.g., points 13 on the 3rd, 8th and 13th floors) and (2) at the mid-span of the floor (e.g., points 1 on the 3rd, 8th and 13th floors). The reason for this selection is that the main beams, as primary load-bearing elements, generally have higher stiffness and can distribute vibrational energy more efficiently, whereas floor slabs are more flexible and prone to local resonance effects.

Comparing these two conditions allows us to evaluate how structural stiffness affects the transmission of vibrational energy in the building.

To study the propagation patterns of vibration waves across different floors, the following test was conducted under condition 3.

Condition 3: the equipment vibration frequency was set to 50 Hz. The equipment excitation was applied sequentially at points 16 (at the mid-span of the floor) and point 17 (at the mid-span of the main beam) on the 13th floor. The acceleration time history at points 16,17 and 25 on floors 8-13 were collected, as shown in Fig. 12

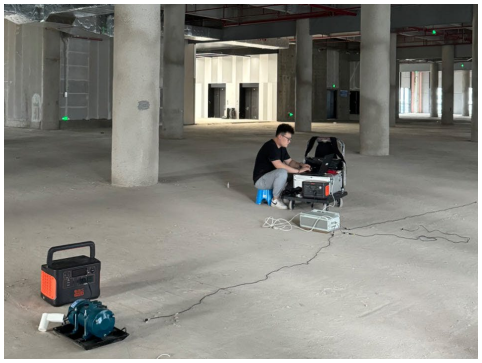

Fig. 12 On-site test

3.3. *Vibration wave propagation test results*

3.3.1. *Modal test results*

To eliminate the interference of high frequencies, the signals of acceleration time history from the heel-drop excitation were processed using a low-pass filter with a cut off frequency of 10 Hz. After filtering, the DC (zero-frequency) components were also removed by subtracting the mean value from the signals. Fig. 13-15 show the acceleration time history and frequency spectrum at points 16-18 on the 3rd, 8th and 13th floors and points 38-40 on the 3rd and 8th floors, respectively under the heel-drop excitation. Based on the frequency spectrum, the first-order vertical natural frequencies are summarized in Table 1.

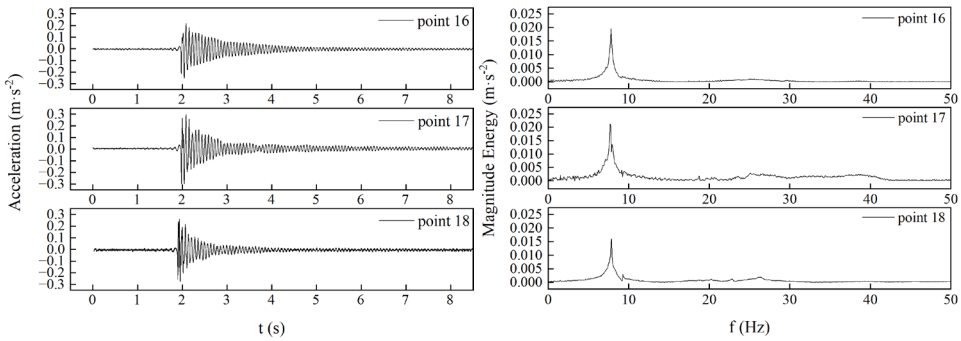

a) acceleration time history curve of points 16-18 b) frequency spectrum curve of points 16-18

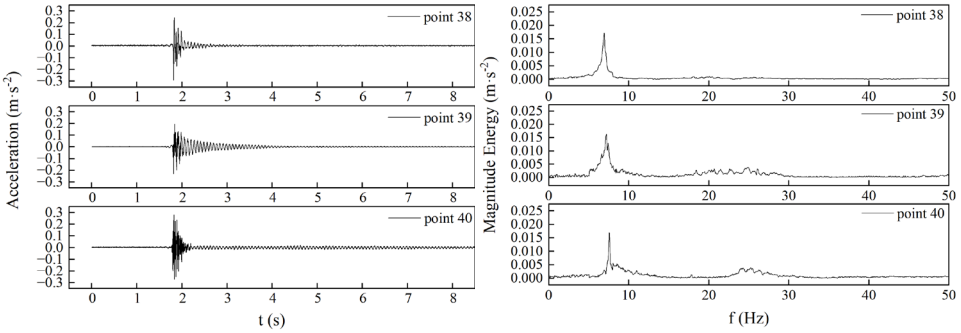

c) acceleration time history curve of points 38-40 d) frequency spectrum curve of points 38-40

Fig. 13 Measuring points curves of the 3rd floor

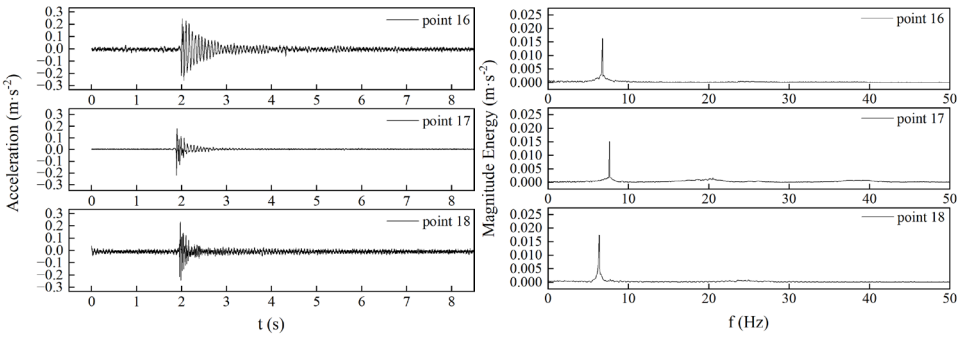

a) acceleration time history curve of points 16-18 b) frequency spectrum curve of points 16-18

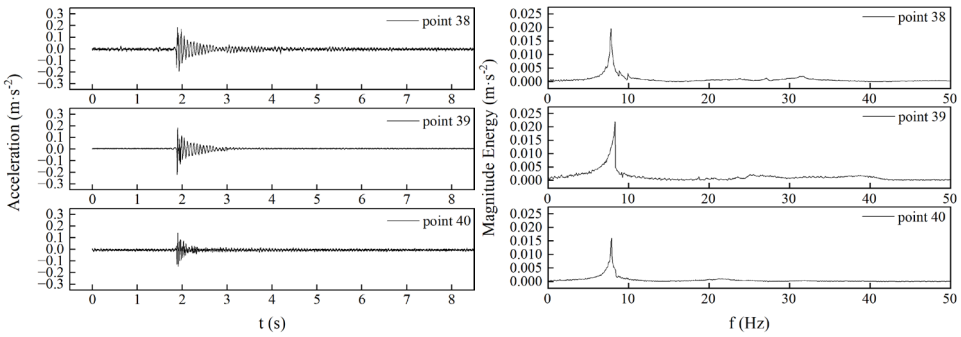

c) acceleration time history curve of points 38-40 d) frequency spectrum curve of points 38-40

Fig. 14 Measuring points curves of the 8th floor

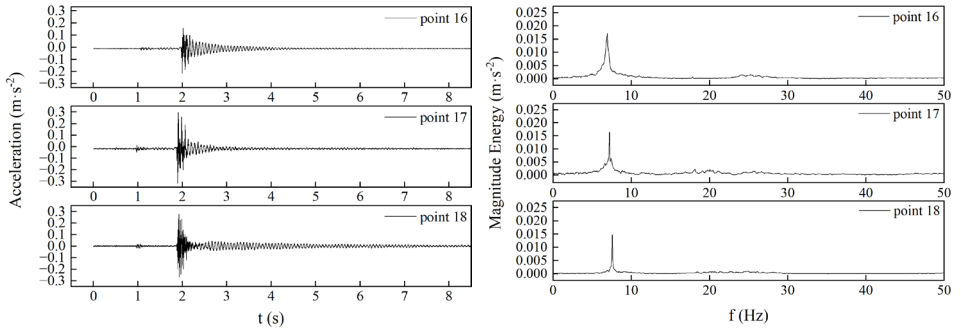

a) acceleration time history curve b) frequency spectrum curve

Fig. 15 Measuring points curves of the 13th floor

From Fig. 13-15 and Table 1, it can be observed that the fundamental frequencies of the floors are between 6-8 Hz. The main reason for the difference is the varying cross-sectional dimensions of the main and secondary beams of each floor, as well as the inevitable experimental errors. However, it is sufficiently accurate for predicting resonance zone of design.

Table 1. First-order vertical natural frequency

Floor	*f* / Hz					
	Zone A			Zone B		
	Point 16	Point 17	Point 18	Point 38	Point 39	Point 40
3rd	7.79	6.65	6.91	6.92	7.19	7.54
8th	7.69	7.62	7.12	7.80	7.89	7.87
13th	7.87	6.98	7.54		NA	

The damping ratios based on the measurement at points 16-18 on the 3rd, 8th and 13th floors and points 38-40 on the 3rd and 8th floors, respectively, were estimated using the half-power bandwidth method. The results are shown in Table 2.

Table 2. Damping ratio of measuring points

Floor	Test point		f_2 / Hz	f_1 / Hz	f_0 / Hz	ξ
3rd	Zone A	16	7.87	7.71	7.79	0.0103
		17	7.77	7.62	7.69	0.0098
		18	7.95	7.80	7.87	0.0095
	Zone B	38	7.03	6.89	6.92	0.1012
		39	7.26	7.11	7.19	0.1043
		40	7.61	7.46	7.54	0.0099
8th	Zone A	16	6.83	6.69	6.75	0.0104
		17	7.70	7.55	7.62	0.0098
		18	7.05	6.91	6.98	0.0100
	Zone B	38	7.87	7.71	7.80	0.1026
		39	7.97	7.81	7.89	0.0095
		40	7.96	7.79	7.87	0.0108
13th	Zone A	16	6.99	6.85	6.91	0.0101
		17	7.26	7.12	7.19	0.0098
		18	7.61	7.47	7.54	0.0093

Note: f_1 and f_2 are the left and right half-power points, respectively. These values correspond to the frequency values at which the spectral amplitude is $1/\sqrt{2}$ of the value at the resonant frequency point. f_0 is the resonant frequency point, and ξ is the structural damping ratio.

From Table 2, it can be observed that the damping ratios estimated based on the response at points 16-18 on the 3rd, 8th and 13th floors and points 38-40 on the 3rd and 8th floors, respectively, are generally around 0.01. Considering that the structural design of each floor is essentially similar, it is assumed, therefore, that the damping ratio is 0.01 for all the floors.

3.3.2. *Vibration test results*

(i) Vibration wave propagation within a floor

Under the test of Condition 1 specified in Section 3.2.2, i.e., the building was subjected to an excitation at point 1 on the 3rd floor, the vibration acceleration time-history and frequency spectrum of points 1-12, 26-31 and point 23 on the same floor are shown in the Fig. 16-17.

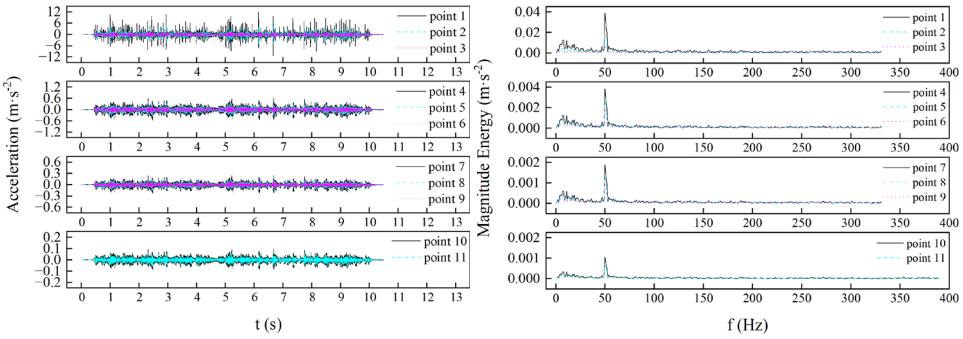

a) acceleration time history curve of points 1–11 b) frequency spectrum curve of points 1–11

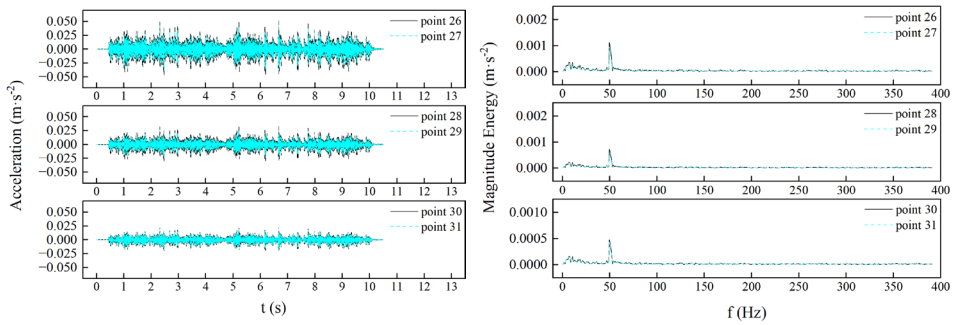

c) acceleration time history curve of points 26-31 d) frequency spectrum curve of points 26–31

Fig. 16 Vibration curves of points 1-11 and points 26-31 of 3rd floor

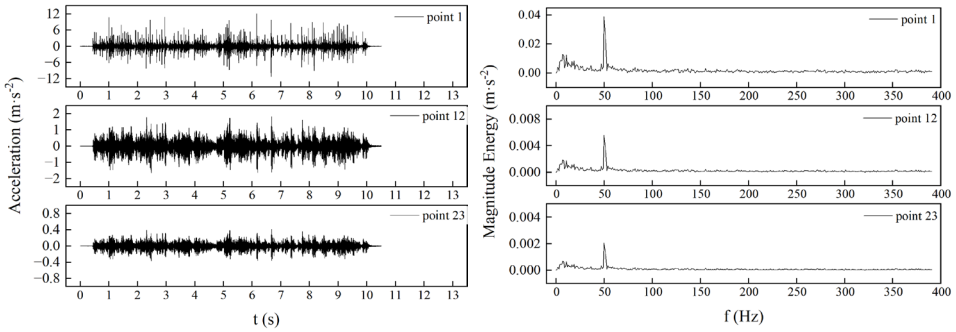

a) acceleration time history curve b) frequency spectrum curve

Fig. 17 Vibration curves of points 1, 12 and point 23 of 3rd floor

The peak vibration acceleration at, points 1-12 and point 23 on the 3rd, 8th and 13th floors and point 26-31 on the 3rd and 8th floors are shown in Table 3.

Table 3. Peak vibration acceleration at points 1-12, 26-31 and point 23

		Test point												
Peak Vibration Acceleration / ($m \cdot s^{-2}$)	Floor		1	2	3	4	5	6	7	8	9	10	11	12	23
	3rd	Zone A	12.014	5.313	2.322	0.611	0.421	0.284	0.244	0.171	0.130	0.094	0.066	1.826	0.407
	8th		12.266	5.054	2.173	0.693	0.487	0.336	0.249	0.178	0.120	0.093	0.063	1.885	0.432
	13th		12.618	5.198	2.351	0.721	0.493	0.355	0.262	0.189	0.136	0.102	0.073	2.081	0.477
	Floor	Zone B	26		27		28		29		30		31		
	3rd		0.051		0.043		0.033		0.027		0.022		0.020		N/A
	8th		0.055		0.046		0.035		0.029		0.025		0.022		

Under test Condition 2, the vibration acceleration time-history and frequency spectrum at points 2, 13-22, 32-37 and point 24 are shown in the Fig. 18-19 when the 3rd floor is subjected to an excitation at point 13.

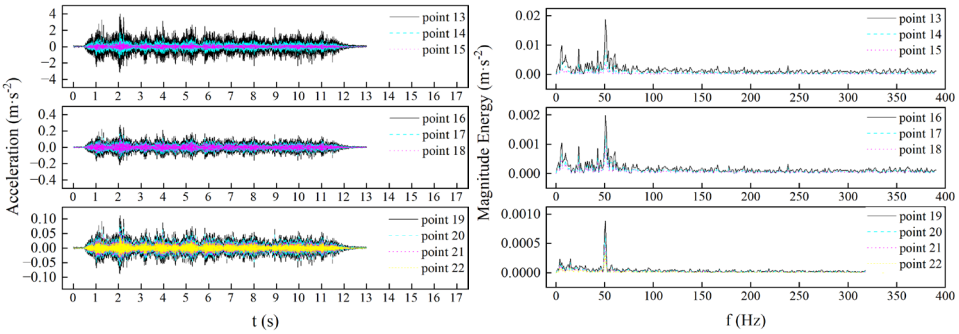

a) acceleration time history curve of points 13-22

b) frequency spectrum curve of points 13-22

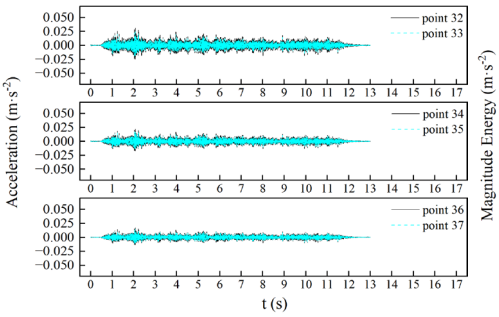

c) acceleration time history curve of points 32-37

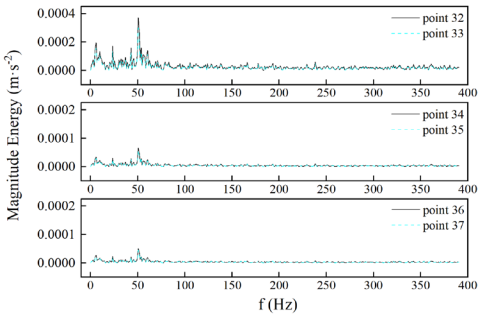

d) frequency spectrum curve of points 32-37

Fig. 18 Vibration curves of points 13–12 and points 32-37 of 3rd floor

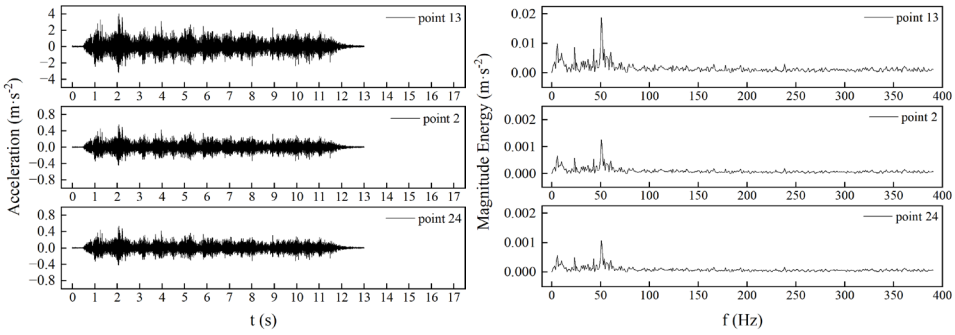

a) acceleration time history curve b) frequency spectrum curve

Fig. 19 Vibration curves of points 2□ 13□ 24 of 3rd floor

352 The peak vibration acceleration at, points 13-24 and point 2 on the 3rd ,8th and 13th
353 floors and points 32-37 on the 3rd and 8th floors are shown in Table 4.

354 Table 4. Peak vibration acceleration at points 13-24, 32-37 and point 2

			Test point											
Peak Vibration Acceleration / (m·s^{-2})	Floor		2	13	14	15	16	17	18	19	20	21	22	24
	3rd	Zone A	0.562	4.031	1.791	0.833	0.275	0.179	0.129	0.112	0.081	0.061	0.042	0.541
	8th		0.517	4.165	1.882	0.875	0.297	0.215	0.152	0.122	0.090	0.066	0.051	0.506
	13th		0.518	4.418	2.085	0.943	0.329	0.238	0.166	0.125	0.092	0.063	0.049	0.520
	Floor	Zone B	32		33		34		35		36		37	
	3rd		0.031		0.025		0.022		0.019		0.017		0.015	
	8th		0.044		0.036		0.029		0.022		0.018		0.016	

355

356 Based on the test results of conditions 1 and 2, it can be found that the vibration
357 response caused by an excitation at the mid-span of a main beam is smaller than that caused
358 by an excitation at the mid-span of a floor, with the former being approximately 35% of
359 the latter. This observation aligns with the expectation that the beams, being stiffer
360 structural elements, distribute excitation force more efficiently, and the middle of the slab
361 experiences more pronounced local vibrations due to its lower stiffness. It is also evident
362 that the vibration response decreases with the increase of the distance from the excitation
363 source.

364 It can be seen from Table 3 that at point 26 of the 3rd and 8th floor, the vibration response
365 exceeds the comfortable rate of acceleration for office occupants,[16] which is about 0.05
366 m·s^{-2}. This indicates that even when the vibration excitation is positioned at the farthest

end of the factory area (Zone A) from the office area (Zone B), the vibration from the factory may still have significant impact on the office area.

If the factory area contains multiple vibration excitations or if the locations of excitation are closer to the office area, the impact on the office space could be far more intensive and deeper into the area. Therefore, it is essential to perform relevant structural vibration analyses to assess the likelihood and severity of any vibration-related health risks and to recommend preventive measures before a factory and an office area within the building are put in to service.

(ii) Vibration wave propagation across different floors

To study wave propagation in different floor caused by the same excitation, Condition 3 in Section 3.2.2 is applied. Under an excitation of point 16 and 17, respectively, on the 13th floor, the vibration acceleration time-history and frequency spectrum of points 16, 17 and point 25 on floors 8-13 are shown in Fig. 20.

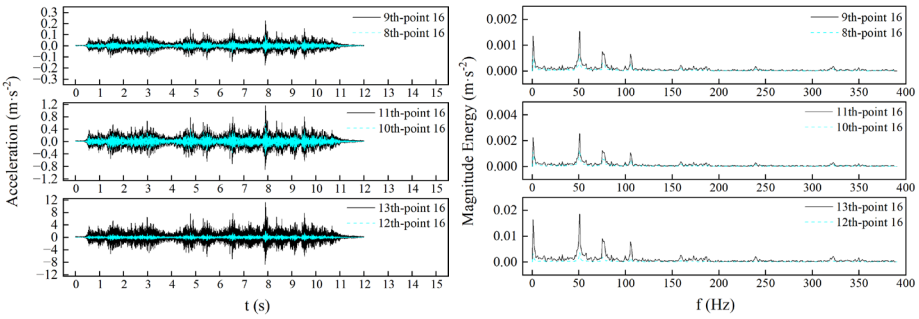

a) acceleration time history curve of point 16 b) frequency spectrum curve of point 16

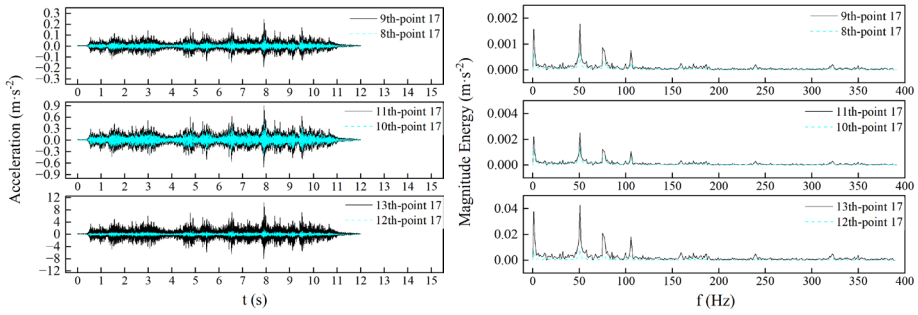

c) acceleration time history curve of point 17 d) frequency spectrum curve of point 17

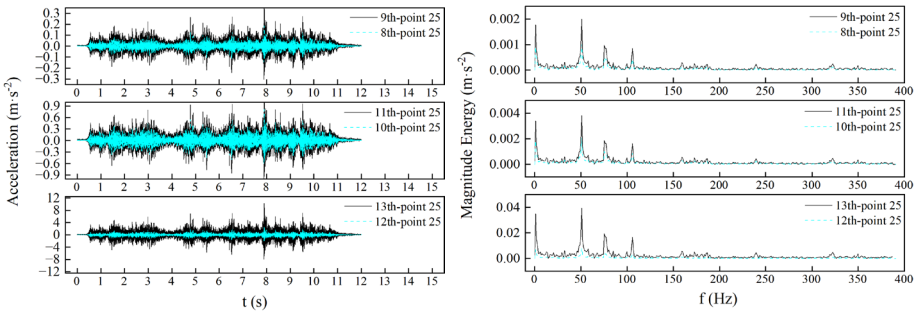

e) acceleration time history curve of point 25 f) frequency spectrum curve of point 25

Fig. 20 Vibration curves of points 16□ 17 and 25 under a 16-point excitation on the 13th floor

The peak vibration acceleration at points 16, 17 and 25 of different floors under the excitations are shown in Table 5.

Table 5. Peak vibration acceleration at points 16, 17 and 25

Excitation point	Test point	Peak acceleration / ($m \cdot s^{-2}$)					
		8^{th} floor	9^{th} floor	10^{th} floor	11^{th} floor	12^{th} floor	13^{th} floor
point 16, floor 13	point 16	0.099	0.227	0.578	1.160	2.244	11.298
	point 17	0.098	0.247	0.518	0.909	2.072	10.428
	point 25	0.129	0.257	0.506	0.936	2.042	10.315
point 17, floor 13	point 16	0.022	0.056	0.173	0.447	1.025	4.379
	point 17	0.029	0.069	0.207	0.511	1.265	4.702
	point 25	0.019	0.048	0.159	0.410	1.024	4.082

Similar to the observations from the vibration under Conditions 1 and 2, under Condition 3, the vibration caused by an excitation at the mid-span of a main beam is also smaller than that caused by the excitation at the mid-span of a floor. From a design perspective, these results suggest that placing vibration-sensitive equipment near a main beam may reduce undesirable vibrations.

3.4. *Comparison between test results and theoretical calculations*

3.4.1. *Comparison of the test and theoretical calculation results when the excitation and response are on the same floor*

Theoretical calculations were performed for the tested building by using the theory presented in Section 2 and following the calculation flow chat (Fig. 7). The calculations were carried out for the same positions of excitation, measurement points, and all other design parameters used in the three test conditions.

The comparison between the test results and the theoretical calculations under Condition 1 are shown in Table 6.

Table 6. Comparison of peak vibration acceleration between test and theory under Condition 1

Test point	Peak Acceleration / ($m \cdot s^{-2}$)								
	3rd floor			8th floor			13th floor		
	Test	Theory	Error (%)	Test	Theory	Error (%)	Test	Theory	Error (%)
1	12.014	11.275	6.151	12.266	12.019	2.014	12.618	12.795	1.403
2	5.313	5.023	5.458	5.054	5.236	3.601	5.198	5.528	6.349
3	2.322	2.249	3.144	2.173	2.416	11.183	2.351	2.678	13.909
4	0.611	0.625	2.291	0.693	0.705	1.732	0.721	0.754	4.577
5	0.421	0.487	15.677	0.487	0.524	7.598	0.493	0.569	15.416
6	0.284	0.305	7.394	0.336	0.348	3.571	0.355	0.394	10.986
7	0.244	0.256	4.918	0.249	0.284	14.056	0.262	0.316	20.611
8	0.171	0.194	13.450	0.178	0.216	21.348	0.189	0.235	24.339
9	0.130	0.124	4.615	0.120	0.146	21.667	0.136	0.167	22.794
	Table 6. (*Continued*)								
10	0.094	0.087	7.447	0.093	0.106	13.978	0.102	0.123	20.588
11	0.065	0.059	9.231	0.063	0.079	25.397	0.073	0.084	15.068
12	1.826	1.795	1.698	1.885	1.978	4.934	2.081	2.136	2.642
23	0.407	0.394	3.194	0.432	0.498	15.278	0.477	0.521	9.224
26	0.051	0.048	5.888	0.055	0.052	5.455			
27	0.043	0.040	6.977	0.046	0.042	8.696			
28	0.033	0.035	6.061	0.035	0.032	8.571	N/A		
29	0.027	0.029	7.407	0.029	0.027	6.897			
30	0.022	0.023	4.545	0.025	0.023	8			
31	0.020	0.021	5	0.022	0.021	4.546			
Average Error (%)	N/A		6.345	N/A		9.922	N/A		12.916

The comparison between the test and theoretical calculations results under Condition 2 are shown in Table 7.

Table 7. Comparison of peak vibration acceleration between test and theory under Condition 2

Test point	Peak Acceleration / ($m \cdot s^{-2}$)								
	3rd floor			8th floor			13th floor		
	Test	Theory	Error (%)	Test	Theory	Error (%)	Test	Theory	Error (%)
2	0.562	0.523	6.940	0.517	0.544	4.963	0.518	0.563	7.993
13	4.031	4.023	0.198	4.165	4.223	1.373	4.418	4.646	4.907
14	1.791	1.675	6.477	1.882	1.845	2.005	2.085	2.146	2.842
15	0.833	0.825	0.960	0.875	0.915	4.372	0.943	1.078	12.523
16	0.275	0.257	6.545	0.297	0.305	2.623	0.329	0.326	0.920
17	0.179	0.195	8.939	0.215	0.225	4.444	0.238	0.246	3.252
18	0.129	0.136	5.426	0.152	0.164	7.317	0.166	0.189	12.169
19	0.112	0.106	5.357	0.122	0.145	15.862	0.125	0.162	22.840

20	0.081	0.092	13.580	0.090	0.102	11.765	0.092	0.125	26.400
21	0.061	0.057	6.557	0.066	0.068	2.941	0.063	0.075	16.000
22	0.042	0.046	9.524	0.051	0.054	5.556	0.049	0.061	19.672
24	0.541	0.479	11.460	0.506	0.525	3.619	0.520	0.579	10.190
32	0.031	0.029	6.452	0.044	0.041	6.818			
33	0.025	0.023	8	0.036	0.035	2.778			
34	0.022	0.020	9.091	0.029	0.027	6.897	N/A		
35	0.019	0.018	5.236	0.022	0.019	13.636			
36	0.017	0.015	11.765	0.018	0.015	16.667			
37	0.015	0.013	13.333	0.016	0.013	18.750			
Average Error (%)	N/A		7.547	N/A		7.355	N/A		11.642

Based on the comparisons for Conditions 1 and 2, it can be found that the error is within 15% for up to 87% (90/103) of the measuring points and the average error is 8.679%.

The errors are attributed to a number of factors, including that

(1) The theoretical model assumes perfectly simply supported boundaries, while in reality elastic constraints exist, minor deviations may exist due to construction tolerances and local stiffness variations.

(2) The assumed material properties, such as Young's modulus and damping ratio, may slightly differ from the actual values due to fabrication inconsistencies, environmental conditions. These variations influence structural stiffness and damping characteristics, leading to localized deviations in vibration response.

3.4.2. *Comparison of the test and the theoretically predicted vibration response of the 8^{th} to 13^{th} floors due to the excitation on the 13^{th} floor excitation*

The comparison between the test results and the theoretical calculations under Condition 3 are shown in Table 8.

Table 8. Comparison of peak vibration acceleration between test and theory

Excitation point	Floor	Peak Acceleration / ($m \cdot s^{-2}$)								
		Point 16			Point 17			Point 25		
		Test	Theory	Error (%)	Test	Theory	Error (%)	Test	Theory	Error (%)
16	8^{th}	0.099	0.103	3.883	0.098	0.127	22.835	0.129	0.154	16.234
	9^{th}	0.227	0.283	19.788	0.247	0.281	12.100	0.257	0.305	15.738
	10^{th}	0.578	0.612	5.556	0.518	0.561	7.665	0.506	0.583	13.208
	11^{th}	1.160	1.239	6.376	0.909	1.082	15.989	0.936	1.067	12.277
	12^{th}	2.244	2.371	5.356	2.072	2.167	4.384	2.042	2.217	7.894
	13^{th}	11.298	11.582	2.452	10.428	10.815	3.578	10.315	10.862	5.036
17	8^{th}	0.022	0.031	29.032	0.029	0.033	12.121	0.019	0.025	24.000
	9^{th}	0.056	0.072	22.222	0.069	0.074	6.757	0.048	0.065	26.154
	10^{th}	0.173	0.201	13.930	0.207	0.229	9.607	0.159	0.187	14.973
	11^{th}	0.447	0.396	12.879	0.511	0.531	3.766	0.410	0.442	7.240

12th	1.025	1.057	3.027	1.265	1.316	3.875	1.024	1.112	7.914
13th	4.379	4.579	4.368	4.702	4.932	4.663	4.082	4.342	5.988
Average Error (%)	N/A		10.739	N/A		8.945	N/A		13.055

Based on the comparison for Condition 3, it can be found that the error is within 15% for up to 75% (27/36) of the points and the average error is 10.913%.

In addition to the aforementioned sources of error, it is also found that the points where relatively large prediction errors occur are almost all on the 8-10th floors that are at least 3 floors away from the excitation, or more than 3 spans away from the excitation on the same floor. The vibration reaching these measurement points is much less intensive, i.e., less than 5% of the vibration of the excitation source, which may reduce the accuracy of the test results. Nevertheless, the overall error between the theory and the experiment is regarded as acceptable.

4. Regression of Vibration Wave Propagation Equation

In this section, we aim to establish a regression model for vibration wave propagation by considering both geometric attenuation and energy loss in the medium. The wave attenuation is influenced by the spatial distance from the excitation source and the material damping properties. A mathematical expression is introduced to characterize the variation of peak acceleration with distance. By fitting theoretical calculation data to this model, the key parameters governing vibration attenuation can be identified. The derived regression equation may be used to predict vibration responses in similar structural environments.

For wave propagation, the primary characteristic is wave attenuation, which is mainly related to the following two aspects

(i) In a three-dimensional space, wave attenuation involves geometric attenuation,[17] where the wave amplitude decreases with the increase of distance r. This can be expressed as

$$A(r) \propto \frac{1}{r^n}, \tag{4.1}$$

where $A(r)$ denotes peak acceleration function.

In this study, the primary focus is on the relationship between the excitation point (X_{exc} , Y_{exc} , Z_{exc}) and the measurement point (X_{meas} , Y_{meas} , Z_{meas}). Therefore, the Euclidean distance is used to define

$$r = \sqrt{(\Delta X)^2 + (\Delta Y)^2 + (\Delta Z)^2} \,, \tag{4.2}$$

where $\Delta X = X_{\text{meas}} - X_{\text{exc}}$, etc.

(ii) In addition to geometric attenuation, energy loss occurs as waves propagate through the medium.[18] This is generally expressed using an exponential factor

$$A(r) \propto e^{-\alpha r} \,, \tag{4.3}$$

where α represents attenuation coefficient, which is associated with the properties of medium, frequency, and damping ratio.

Combining the two aspects mentioned above, the expression of wave amplitude considering both geometric attenuation and energy loss is

$$A(r) \approx \frac{\beta_0}{r^n} e^{-\alpha r} \,, \tag{4.4}$$

where β_0 represents the initial amplitude.

Eq. (4.4) can be further modified and expressed as

$$A_{\text{peak}}(r) = \frac{\beta_0}{(r + \beta_1)^n} e^{-\beta_2 r} \,, \tag{4.5}$$

where A_{peak} is the peak acceleration at a Euclidean distance r from the excitation source, with the unit of m·s-2; β_1 is the "starting distance" correction, primarily to prevent the unrealistic situation where the amplitude tends to infinity as $r \to 0$; n is the control parameter for the overall attenuation rate; β_2 is attenuation coefficient. β_0 , β_1 , β_2 and n can be estimated through data fitting using nonlinear regression.

The validated theoretical calculation method presented in Section 2 is used to obtain peak accelerations at various points located at different distances from the excitation source within the structure. These data are then used to fit the parameters in Eq. (4.5) mentioned above.

The accuracy of the regression model depends on the selection of data points. To ensure a systematic and representative dataset, a four-factors orthogonal design L36 ($3^3 \times 2^2$) is employed to prepare the data set:

(1) Factor A: the floor of excitation. In this study, three floors, i.e., the 3rd, 8th and 13th floors are considered.

(2) Factor B: position of excitation on a floor. In this study, mid-span of the floor (point 20) and mid-span of the beam (point 21) are considered.

(3) Factor C: floor response. In this study, three ranges of floor, i.e., floors 1-4, floors 5-9 and floors 10-13 are considered to represent, respectively, the lower, middle and upper floors.

(4) Factor D: position of response on a floor. In this study, mid-span of a floor (centre of each floor panel) and mid-span of a beam (centre of each beam) are considered.

Amongst the 36 datasets from the theoretical calculations, 29 of them were used in the fitting process, and the remaining 7 (about 20% of 36) independent sets were used to validate the regression model. The comparisons between the predictions acceleration calculated from the theoretical model and the regression model are shown in Table 9. The mean square error (MSE), mean relative error and R^2 of the comparisons are, respectively 0.0012 m·s^{-2}, 3.18% and 0.985, demonstrating that the regression model is sufficiently accurate.

Table 9. Comparison between the WPA and the regression model

Excitation point	Response point	Computational value (m·s^{-2})	Predicted value (m·s^{-2})	Absolute error	Relative error (%)
Point 20 of 3th floor	Point 20 of 3th floor	11.573	11.486	0.087	0.75
Point 20 of 3th floor	Point 21 of 3th floor	5.345	5.327	0.018	0.34
…	…	…	…	…	…
Mean	N/A	N/A	N/A	0.043	3.18
MSE(m·s^{-2})	N/A	N/A	N/A	0.0012	N/A
R^2	N/A	N/A	N/A	0.985	N/A

This design ensures a representative coverage of both excitation and response locations across the full height of the structure. The fitted parameters are shown in Table 10.

Table 10. Parameter estimation under different conditions

Excitation floor	Excitation point Location	β_0	β_1	β_2	n	MSE(m·s^{-2})	R^2
3rd, 8th and 13th	Point 20	24.276	305.791	0.168327	0.1315743	1.021	0.9256
	Point 21	7.426	254.325	0.182164	0.04351785	0.426	0.8463

From Table 10, the MSE is 1.021 (0.426), indicating a small error between the predicted and computational data and a good model fit. The R^2 is 0.9256 (0.8463), showing that the model explains 92.56% (84.63%) of the data variance, demonstrating excellent fitting performance.

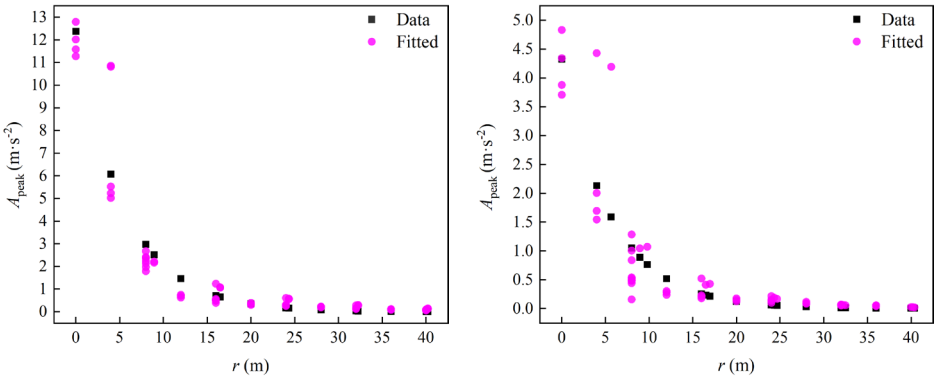

a) excitation point at the mid-span of the floor b) excitation point at the mid-span of the beam

Fig.21 Comparison of fitted model and data used in the fitting

Fig.21 shows the comparison between the fitted model and the data used in the fitting. It can be observed that the model predicts the attenuation trend at a medium or long distances ($r > 10$ m) well. The error between the magenta points (predicted values) and the black points (discrete test data) is small, and the model fits the data within the range effectively. However, there is an increased deviation in the fitting of short distances. This deviation is not a focus of this study, as the purpose of the research is to explore the propagation of vibration waves between different functional areas and floors to understand the impact of vibration in high-rise multifunctional buildings. When the distance between the point of response and the excitation point is too short, the vibration response is similar to the excitation, making it less significant for practical research.

The proposed regression formula (4.5) is derived based on fundamental vibration propagation principles, considering both geometric attenuation and material damping. The key parameters (e.g., β_0, β_1, β_2 and n) can be recalibrated for different structural configurations without altering the structure of the formulation. The regression model can be adapted to different high-rise composite structure configurations by recalibrating the key parameters using new datasets. If the structural properties or boundary conditions

change, the model can be updated through additional regression analyses without modifying the fundamental mathematical structure.

5. Conclusions

This study presents a new WPA calculation method for predicting vibration responses in high-rise steel-concrete composite industrial buildings. The method was validated by the results of on-site tests on the Pingshan new energy vehicle industrial building 3A, a high-rise composite structure building in Shenzhen. Based on the framework of vibration wave propagation that considers wave attenuation, a regression equation for predicting vibration wave propagation was proposed and calibrated through data fitting. From this study, the following conclusions are drawn:

- The placement of equipment has significant impacts on vibration.

The vibration caused by an excitation at the mid-span of a main beam is smaller than that caused by excitation at the mid-span of a floor slab, with the former being approximately 35% of the latter. Thus, for improved vibration control and occupant comfort, it is recommended to locate equipment on main beams whenever possible.

- The derived regression equation can satisfactorily predict vibration responses at locations that have a mid-to-long-distance to the excitation.
- This study focuses on a specific type of high-rise composite structure, and the regression model was calibrated for this scenario. Future research is required to extend this model to account for variations in structural configurations by incorporating additional influencing factors such as floor stiffness and column density.

This work contributes to fulfilling a critical research gap in modelling vibration propagation in high-rise composite multifunctional industrial buildings. The proposed regression has the potential to be developed further for adoption in practical design of high-rise and multifunctional steel-concrete composite structures under equipment-induced vibrations.

Acknowledgments

This work supported by the Natural Science Foundation of China (No. 52178129), Science and Technology Planning Project of Shenzhen Municipality (GJHZ20220913143007013) and Science and Technology Planning Project of Shenzhen Municipality (KCXST20221021111408021).

References

1. A. Ebrahimpour and R.L. SACK, Modeling dynamic occupant loads. *J. Struct Eng.* **115**(6) (1989) 1476–1496.
2. F. Gasella, Semi-active hydraulic structural control, in *Proc. Proceedings of the International Workshop on Structural Control,* Hawaii, United States (August 1993), pp. 9305–9311.
3. P. Li and L.W. Peng, Analysis on vibration coupling effect and structural strengthening of a mill building. *J. Building Struct*, **40**(02) (2010) 77–80.
4. B.F. Spencer, S.J. Dyke, M.K. Sain, and J.D Carlson, Phenomenological model for magnetorheological dampers. *J. Eng. Mech.* **123**(1993) 230–238.
5. Y.T. Lung, Control of Seismic-excited Buildings Using Active Variable Stiffness Systems. *J. Eng Struct*, **18**(8) (1996) 589–596.
6. D. Gerardo and T.G. Amador, Prediction of the Influence of Higher Modes on the Dynamic Response of High-Rise Buildings Subjected to Narrow-Banded Ground Motions. *J. Int J Struct Stab Dy,* **23**(04) (2023) 1–24.
7. Y.X. Wu, Q.H. Pu and W.J. Luo et al, Research on Vibration and Secondary Noise Characteristics of Sensitive Buildings Along Metro Lines Induced by Metro Operation. *J. Int J Struct Stab Dy,* **31**(06) (2024) 17–43.
8. Z.H. Zhang and Q. Li, Dynamic Analysis of a 600-m-High Supertall Building Subjected to Long-Period Ground Motions, Ordinary Ground Motions and a Super Typhoon: A Comparative Study. *J. Int J Struct Stab Dy,* **17**(10) (2024) 10–37.
9. C.J. Wu and R.G. White, Vibrational power transmission in a multi-supported beam. *J. Sound Vib* ,**181**(1) (1995) 99–114.
10. Y.K. Tso and C.H. Hansen, Wave propagation through cylinder/plate junctions. *J. Sound Vib*, **186**(3) (1995) 447–461.
11. Q. He and Z. He, Transverse Vibration of an axially moving beam with fixed support by wave propagation. *J. Noise Vib Control*, **01** (2007) 41–44.
12. M.X. Chen, C. Zhang and N.Q. Deng. Solving the vibration of a cylindrical shell with end - plates in water under low - frequency excitation by the wave propagation method. *J. Vib Eng*, 2014, **27**(6) (2014) 842–851.
13. H.J. Zhou, C.C. He and W.Y. Li, Application of wave propagation method to vibration analysis of rod-and-beam structures with arbitrary boundary conditions. *J. Noise Vib Control*, **35**(2) (2015) 32–35.
14. C.J. Wu, Wave Propagation Approach for Structural Vibration (Springer Publications ,2021).
15. C.J. Wu, Z.G. Chen and Z.Y. Xu, Harmonic response of longitudinal vibration for uniform finite rods with WPA method, in *Proc. Proceedings of the 2005 Academic Conference on Ship Structural Mechanics*, Beijing, China (July 2005), pp. 456–462.
16. Technical standard for vibration comfort of building floor structures: JGJ/T 441-2019. (China Architecture and Building Press, 2019).
17. V. Graizer, Geometric spreading and apparent anelastic attenuation of response spectral accelerations. *J. Soil Dyn Earthq Eng*, **162** (2022) 172–176.

18. C. Ramadas, K. Balasubramaniam, A. Hood, M. Joshi and C.V. Krishnamurthy, Modelling of attenuation of lamb waves using rayleigh damping: numerical and experimental studies. *J. Compos Struct*, **93**(8) (2011) 2020–2025.